MetaResource vol. XX, no. X, pp. 1–XX, 202X
DOI: 10.23919/METAR.2026.000057
Original Article

Process optimization and mechanism study of cementitious material prepared from coal gangue via hydrothermal-calcinations synergistic activation

Tingye Qi[1,2,3,4,5,✉], Tian Qiu[1,2,3,4], Xin Cheng[1,2,3,4], Jiawei Wang[1,2,3,4], Liuyuanxiang He[1,2,3,4], and Senlin Yi[1,2,3,4]

[1] *College of Mining Engineering, Taiyuan University of Technology, Taiyuan 030024, China*
[2] *Shanxi Province Research Center of Green Mining Engineering Technology, Taiyuan 030024, China*
[3] *Shanxi Coal-based Resources Green-efficient Mining Engineering Research Center, Taiyuan 030024, China*
[4] *Key Laboratory of Shanxi Province for Mine Rock Strata Control and Disaster Prevention, Taiyuan 030024, China*
[5] *Shanxi-Zheda Institute of Advanced Materials and Chemical Engineering, Taiyuan 030024, China*

Received: 12 Dec 2025
Revised: 26 Feb 2026
Accepted: 9 Mar 2026
Online: xx xxx xxxx

KEYWORDS

coal gangue,
cementitious material,
hydrothermal synthesis,
orthogonal test,
microstructure

ABSTRACT

To enable efficient valorization of bulk industrial solid waste, coal gangue cementitious materials (CGCM) were synthesized via hydrothermal treatment and low-temperature calcination. Using an orthogonal experimental design, the effects of hydrothermal temperature (*A*), Ca/Si molar ratio (*B*), NaOH content (*C*), and calcination temperature (*D*) on material performance were evaluated, with 28-day compressive strength as the key response for range analysis. The influence ranking of factors on strength was $D > B > A > C$. Optimal parameters—hydrothermal temperature of 90 °C, Ca/Si ratio of 2.0, NaOH content of 1.5%, and calcination temperature of 800 °C—yielded a 28-day compressive strength of 19.3 MPa. Based on orthogonal experiment results, the influence of calcination temperature and Ca/Si ratio on material microstructure and properties was examined. Low-temperature calcination at 800 °C favors formation of highly active phases (β-C_2S, α'H-C_2S, CA, and $C_{12}A_7$), whereas 1,000 °C promotes inert C_2AS generation, sharply reducing strength. The Ca/Si ratio governs active mineral formation by modulating silicate polymerization. Conductivity and pH tests confirmed optimal ion dissolution and pozzolanic reactivity at 800 °C, underpinning strength development. This study provides a high-value utilization pathway for coal gangue and elucidates micro-level mechanisms supporting mine backfilling applications.

Address correspondence to Tingye Qi: qty198402@163.com

有斜出版 YOUKE PUBLISHING EXCLUSIVELY AVAILABLE VIA IEEE Xplore DIGITAL LIBRARY

1 Introduction

Ongoing coal extraction in China has generated over 7 billion tons of coal gangue—a major industrial solid waste—with annual additions exceeding 100 million tons [1]. The vast accumulation of coal gangue not only occupies land resources but also triggers environmental issues, including air and water pollution, as well as geological hazards. Its disposal and valorization thus remain critical challenges [2–4].

The vast accumulation of coal gangue not only occupies land resources but also triggers environmental issues, including air and water pollution, as well as geological hazards. Its disposal and valorization thus remain critical challenges [5, 6]. Composed mainly of SiO_2 and Al_2O_3, coal gangue chemically resembles natural volcanic ash and thus holds theoretical potential for cementitious material preparation; however, its pristine mineral structure is stable [7]. Coal gangue possesses a stable mineral structure, resulting in low pozzolanic activity. Its reactivity when directly blended with cement is considerably lower than that of conventional supplements like slag or fly ash, thus necessitating activation to disrupt the stable lattice and unlock its latent reactivity.

At present, the common methods of activating coal gangue mainly include mechanical grinding activation [8], thermal activation [9], and chemical activation [10]. Mechanical grinding mainly improves the activity by increasing the specific surface area [8]. Thermal activation via high-temperature calcination disrupts the crystal lattice of coal gangue, with temperature being the critical determinant of reactivity. Calcination within the 650–800 °C range induces dehydroxylation of minerals like kaolinite into amorphous metakaolinite, thereby significantly enhancing pozzolanic activity [9]. Chemical activation typically employs alkali activators (e.g., NaOH, water glass) to establish an alkaline, OH^--rich environment, thereby facilitating the depolymerization and subsequent reorganization of silicon-oxygen and aluminum-oxygen tetrahedra [10]. As an effective pretreatment, the hydrothermal method facilitates the dissolution and reconstruction of the silicon-aluminum phase at relatively low temperatures, thereby creating favorable conditions for subsequent activation [11–13].

While various activation methods have been explored, single approaches often yield limited efficacy. Consequently, combined strategies (e.g., mechanical-thermal, thermal-chemical activation) have emerged as more effective routes. Nevertheless, studies on synergistic activation of coal gangue via hydrothermal pretreatment coupled with low-temperature calcination remain scarce, particularly regarding its cementitious performance and underlying mechanisms.

This study proposes a synergistic activation process integrating hydrothermal pretreatment and low-temperature calcination to prepare coal gangue cementitious materials (CGCM). An orthogonal experimental design was employed to systematically investigate the effects of hydrothermal temperature, Ca/Si molar ratio, NaOH content, and calcination temperature on material activity, enabling the identification of optimal preparation parameters. The resulting materials were characterized via X-ray diffraction (XRD), scanning electron microscopy (SEM), and measurements of conductivity and pH to analyze phase composition, microstructure, and pozzolanic reaction kinetics. Compressive strength, rheological behavior, and setting properties were also evaluated. This work offers both a novel technical approach and a theoretical foundation for the high-value utilization of coal gangue, contributing to the green and sustainable transformation of the coal industry.

2 Materials and methods

2.1 Material preparation

The coal gangue used in this study was taken from a mine in the south of Taiyuan, and its chemical composition was analyzed by X-ray fluorescence spectroscopy (XRF) as shown in Table 1. It is mainly composed of SiO_2 (55.56%) and Al_2O_3 (31.00%), and contains a small amount of Fe_2O_3, CaO, K_2O, and so on. Other chemical reagents used in the experiment were analytically pure reagents from Sinopharm Group Chemical Reagents Co., Ltd., China, including calcium hydroxide ($Ca(OH)_2$, purity ≥ 99%) and sodium hydroxide (NaOH, purity ≥ 98%), which were used to provide a calcium source and alkaline environment.

Table 1 XRF test results for coal gangue powder

Raw material	SiO_2	Fe_2O_3	Al_2O_3	CaO	MgO	K_2O	TiO_2	Na_2O	P_2O_5	LOI
Coal gangue	55.56	4.94	31.00	2.12	0.02	1.63	0.85	0.38	0.06	18.12

As shown in Figure 1(a), particle size analysis indicated over half of the powder was below 60 μm; the specific surface area of coal gangue powder measured by Brunauer–Emmett–Teller (BET) is 359 m^2/g, providing sufficient reactivity for subsequent activation. The XRD pattern in Figure 1(b) revealed quartz (main peak at 26.6°) and kaolinite (peaks at 22.3° and 24.9°) as the primary crystalline phases. Kaolinite serves as the main clay mineral for the key phase of target phase transformation and reactivity enhancement [14, 15]. SEM in Figures 1(c) and 1(d) revealed irregular particles with smooth, dense surfaces and typical lamellar stacking of kaolinite, alongside quartz particles [16]. This dense, crystalline microstructure explains the inherently low pozzolanic activity of raw coal gangue and underscores the necessity of activation.

To optimize the preparation process, four key factors, hydrothermal temperature (*A*), Ca/Si molar ratio (*B*), NaOH content (*C*), and calcination temperature (*D*), were selected. Each factor was set at three levels, as shown in Table 2. The $L_9(3^4)$ orthogonal test design is shown in Table 3. Taking the compressive strength of 28-day mortar as the index, the significance of each factor and the optimal process combination are determined by the range analysis method.

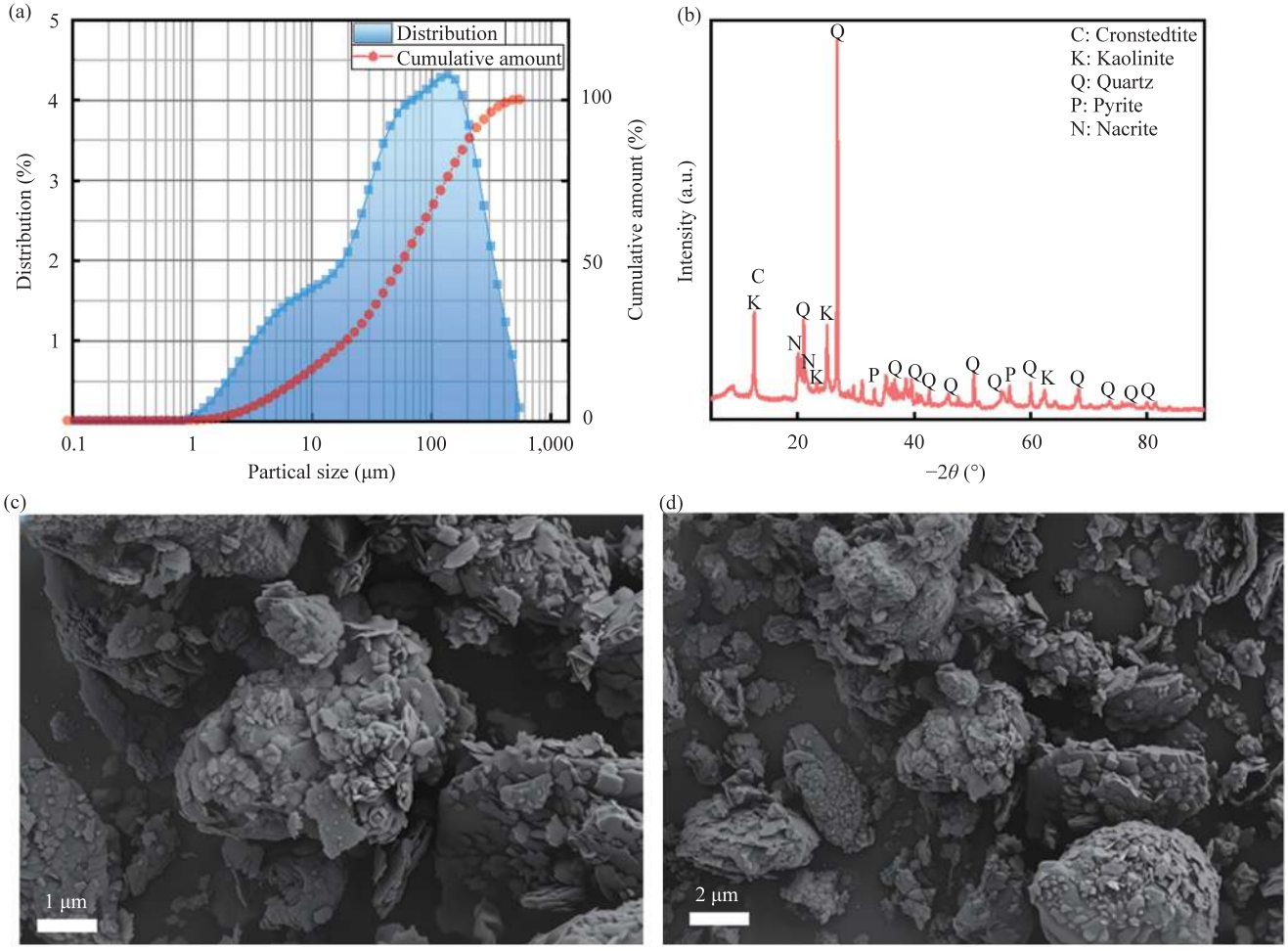

Figure 1 Particle size analysis, mineral composition, and microstructure of coal gangue: (a) particle size analysis, (b) mineral composition, and (c) microstructure

Table 2 Factor level and coding of an orthogonal experiment

Level	*A* (°C)	*B*	*C*	*D* (°C)
−1	60	1.5	1	600
0	90	2	1.5	800
1	120	2.5	2	1,000

Table 3 Orthogonal experimental design and results

Group	A	B	C	D	R
1	−1	−1	−1	−1	7.2
2	−1	0	1	0	15.5
3	−1	1	0	1	3.5
4	0	−1	1	1	2.4
5	0	0	0	−1	15.4
6	0	1	−1	0	16.6
7	1	−1	0	0	18.9
8	1	0	−1	1	2.8
9	1	1	1	−1	10

Note: The compressive strength unit is MPa.

2.2 Test method

2.2.1 Mortar strength test

According to the national standard GB/T 17671-1999 cement mortar strength test method (ISO method), cement mortar specimens with a size of 40 mm × 40 mm × 160 mm were prepared. After curing to a specified age under standard curing conditions, the 28 day compressive strength was measured by a servo-controlled machine.

2.2.2 Microstructure characterization

The phase composition of the material was analyzed by an XRD (MiniFlex600). The scanning range (2θ) was 5°–90°, and the scanning rate was 2 (°)/min. The microstructure and structural characteristics of the samples were observed by an SEM (Regulus 8100, Hitachi, Japan). The acceleration voltage was 5 kV. The samples were sprayed with gold before the test to improve the conductivity.

2.2.3 Flow performance

The apparent viscosity of the fresh paste was measured using a rotary rheometer (Anton Paar) with a shear rate range of 0.1–100 s^{-1}. The setting time of cement paste was determined according to GB/T 1346-2011 cement standard consistency water consumption, setting time, and stability test method. The standard slump tube was used to evaluate the flow performance of fresh slurry, and the slump expansion diameter was recorded to determine the flow performance of the slurry.

2.2.4 Pozzolanic activity

In order to evaluate the pozzolanic activity of the cementitious material, 1.0 g of the sample powder was added to 100 mL of deionized water and magnetically stirred at a constant speed at a constant temperature ((25±1) °C). The dynamic evolution of conductivity and pH value during the reaction was monitored by conductivity meter and pH meter, respectively. The conductivity was measured every 50 min from the beginning of the reaction to 350 min. The pH value was measured every 2 h and continuously monitored for 16 h to systematically investigate the process of pozzolanic reaction.

3 Results and analysis

3.1 Orthogonal test analysis

Range analysis of the orthogonal test results (Table 3) was performed, with the calculated range (R) values for each factor summarized in Table 4. K represents the sum of the test results at each level of a given factor, while k is the average value of K divided by the number of repetitions at that level. The range R, calculated as the difference between the maximum and

Table 4 The range analysis results of the compressive strength regression equation

Factors	*A*	*B*	*C*	*D*
$\bar{K}1$	28.6	26.6	28.5	32.6
$\bar{K}2$	34.4	37.8	33.7	51
$\bar{K}3$	31.7	27.9	30.1	8.7
$\bar{k}1$	9.53	8.87	9.5	10.87
$\bar{k}2$	11.47	12.6	11.23	17
$\bar{k}3$	10.43	9.3	10.03	2.9
R	1.94	3.73	1.73	14.1
Significance size	$D > B > A > C$			

Note: K is the sum of each level index and k is the mean of each level index; range $R = \max(k) - \min(k)$; all strength data units are in MPa.

minimum *k* values.

The *R* value reflects the relative significance of each factor on the activation efficacy of CGCM: A larger *R* indicates a more pronounced influence. The obtained ranges followed the order $R(D) > R(B) > R(A) > R(C)$, establishing the following hierarchy of factor importance: calcination temperature (*D*) > Ca/Si molar ratio (*B*) > alkali activator content (*A*) > liquid–solid ratio (*C*). Notably, calcination temperature and Ca/Si ratio emerged as the two dominant factors governing the properties of the resulting cementitious material.

The theoretical optimal parameter combination was determined by comparing the mean value (*k*) of the response at each factor level. This analysis identified the optimal conditions as: hydrothermal temperature of 90 °C, Ca/Si molar ratio of 2.0, NaOH content of 1.5%, and calcination temperature of 800 °C. Under these conditions, the resulting material exhibited a maximum 28-day compressive strength of 19.3 MPa.

In order to confirm the synergistic effect of hydrothermal-calcination, the cementitious material was prepared by one-step calcination method, that is, the raw materials were treated under the same calcination conditions, but no hydrothermal treatment was carried out. The specific surface area, density, and compressive strength of mortar at 28 day age were compared between the one-step calcination method and the optimal group. The results are shown in Table 5. The results show that the optimal group of hydrothermal synthesis-low temperature calcination is significantly better than the control group in strength index, thus verifying the effectiveness of synergistic activation.

3.2 Microstructure analysis

3.2.1 XRD

Based on the orthogonal test results (Table 3), the effects of the two dominant factors—calcination temperature and Ca/Si molar ratio—on the phase evolution and strength development of CGCM were systematically analyzed.

Figure 2 reveals significant differences in clinker phase composition across calcination temperatures. At 600 °C, the main gelling phases are β-C_2S and CA. At 800 °C, α′H-C_2S and $C_{12}A_7$ additionally appear, accompanied by the highest diffraction intensities of β-C_2S and α′H-C_2S, indicating their abundance as key strength-contributing phases. This compositional evolution correlates with superior compressive strength at all ages for samples calcined at 800 °C. Notably, the formation of α′H-C_2S occurs at a lower temperature than in conventional synthesis, attributed to stabilization by Na^+ and K^+ ions incorporated from coal gangue during hydrothermal reaction. Further increasing the calcination temperature to 1,000 °C induces a marked phase transformation, with gehlenite (C_2AS), α′H-C_2S, and CA_2 becoming the dominant phases in the clinker. The pronounced diffraction intensity of gehlenite in the XRD patterns indicates its abundance; as an inert phase, its formation substantially diminishes clinker reactivity. This transformation proceeds via reaction (1): $CaO + SiO_2 + CA \rightarrow C_2AS$ [17–19]. Cementitious properties diminish at elevated temperatures. The absence of $Ca(OH)_2$ peaks confirms its complete decomposition below 600 °C. As the temperature rises, progressive decarbonation is evidenced by weakening $CaCO_3$ peaks alongside intensifying CaO reflections, approaching completion at 1,000 °C. Concurrently, the diminished intensity of $C_{12}A_7$ suggests the onset of its decomposition at this temperature.

$$CaAl_2O_4 + CaO + SiO_2 \rightarrow Ca_2Al_2SiO_7 \quad (1)$$

Table 3 reveals that the compressive strength of CGCM first increases and then decreases with rising Ca/Si molar ratio. Within the range of 1.5–2.0, strength enhancement correlates positively with Ca/Si ratio, attributable to progressive formation of $C_{12}A_7$—as evidenced by its intensifying XRD peaks. As a highly

Table 5 Related properties of cementitious materials in the optimal group and the control group

Group	BET specific surface area (m^2/g)	Blaine specific surface area (m^2/g)	Density (g/cm^3)	28 day compressive strength (MPa)
Optimal group	942.5	396.5	3.2	19.3
One-step calcination	831.7	371.8	3.3	10.4

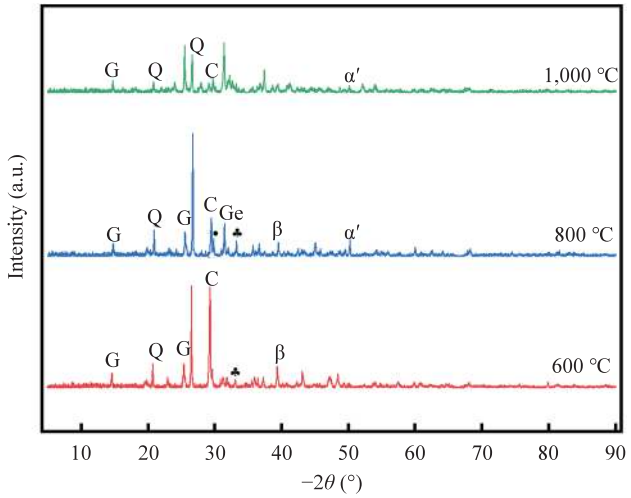

Figure 2 XRD patterns of clinker at different calcination temperatures (Q: Quartz; C: $CaCO_3$; •: $C_{12}A_7$; ♣: CA; Ge: Gehlenite; G: $CaSO_4$)

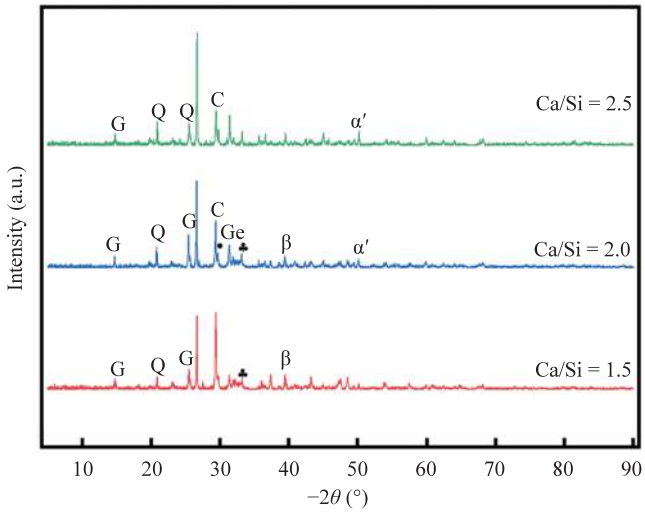

Figure 3 XRD patterns of clinker under different Ca/Si molar ratios (Q: Quartz; C: $CaCO_3$; •: $C_{12}A_7$; ♣: CA; Ge: Gehlenite; G: $CaSO_4$)

hydraulic phase, $C_{12}A_7$ constitutes a key strength contributor within the cementitious system [20, 21]. Increased Ca^{2+} content reduces bridging oxygen within the silicon–oxygen network, shortening silicate tetrahedral chains and lowering polymerization—thereby promoting active calcium silicate formation. Belite (C_2S), the primary cementitious phase in clinker, subsequently hydrates to generate $Ca(OH)_2$, which further participates in the formation of ettringite and C–S–H gel [17, 22]. Increasing the Ca/Si molar ratio elevates the content of tobermorite and calcium hydroxide in the synthesized products, thereby promoting early-age strength development of the material.

3.2.2 SEM

Figure 4 illustrates the microstructural evolution of clinkers with calcination temperature. At 600 °C, the clinker exhibits dense blocks and nascent spheres with blurred boundaries, indicative of incomplete organic decomposition and limited mineral transformation. This dense morphology restricts pore development, resulting in low specific surface area that hinders ion dissolution and reactant transport during hydration. At 800 °C, the microstructure becomes markedly more porous: Particle morphology regularizes and interparticle spacing widens, forming a loose, interconnected network conducive to subsequent hydration reactions. This porous microstructure arises from two concurrent processes: carbonate decomposition and volatile release create intraparticle voids, while solid-state formation of nanoscale active phases (β-C_2S, α′H-C_2S) introduces additional porosity through loose particle packing. Such interconnected porosity facilitates water infiltration and ion transport, accelerating early hydration and providing sufficient space for hydration products to develop into a dense, interwoven matrix—ultimately yielding maximum 28-day strength. At 1,000 °C, however, partial sintering induces pore

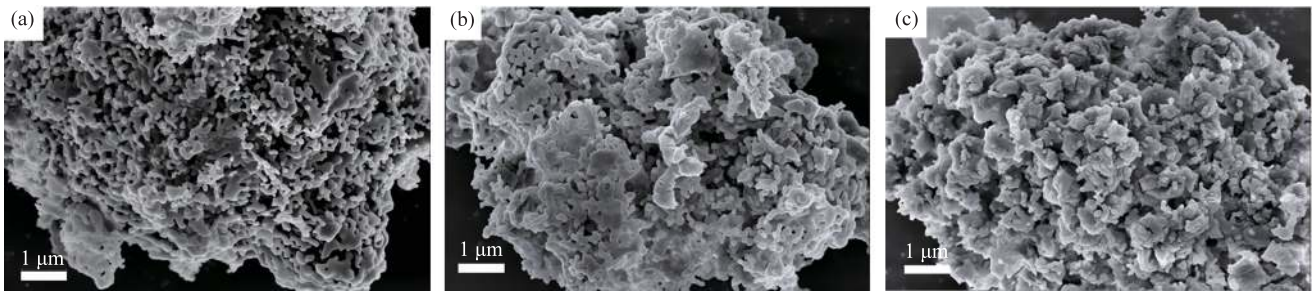

Figure 4 SEM diagram of clinker at different calcination temperatures: (a) 600 °C, (b) 800 °C, and (c) 1,000 °C

collapse and densification, coinciding with gehlenite (C_2AS) formation. As an inert phase detected by XRD, gehlenite encapsulates active particles, thereby diminishing overall reactivity.

Figure 5 illustrates the influence of Ca/Si molar ratio on clinker morphology. At a ratio of 1.5, the clinker consists of fine granular or spherical aggregates arranged in "grape-string" or "honeycomb" formations, characterized by rough surfaces and high porosity. Increasing the ratio to 2.0 yields localized "cauliflower-like" microcrystalline aggregates—indicative of the C–S–H to C_2S transition—accompanied by reduced porosity, enhanced interparticle connection, and greater densification. This suggests that an optimal calcium content promotes silicon–oxygen network polycondensation and facilitates the formation of higher-crystallinity silicate phases upon calcination. At a ratio of 2.5, however, large cubic or square crystals—identified as free CaO (f-CaO)—appear, exhibiting poor interfacial bonding, common microcracks and voids, structural loosening, and localized spalling.

3.3 Study on the properties of cementitious materials

3.3.1 Slurry viscosity

As shown in Figure 6, mortar viscosity decreases with calcination temperature from 600 to 800 °C, reaching a minimum of 1.34 Pa·s, before increasing slightly up to 1,000 °C. This trend is attributed to temperature-dependent changes in clinker composition and microstructure. Compared to 600 °C, more complete combustion of residual carbon in coal gangue occurs at 800 °C. Since carbon exhibits high water absorption, its consumption liberates free water and reduces water film thickness, thereby lowering viscosity. Beyond 800 °C, partial sintering and phase transformation offset this effect, leading to a marginal viscosity increase [23]. At 1,000 °C, increased specific surface area, structural defects, and bond breakage generate highly active particles with enhanced water adsorption. These particles intensify van der Waals attraction while weakening electrostatic repulsion, thereby promoting pozzolanic reactions. The resulting formation of additional cementitious products leads to a net increase in viscosity [24–26].

As the Ca/Si molar ratio increases from 1.5 to 2.5, the viscosity of the CGCM paste rises gradually, peaking at 1.65 Pa·s when Ca/Si = 2.5. This trend is governed by two primary mechanisms. First, as a divalent cation with large ionic radius and low charge density, Ca^{2+} readily coordinates with oxygen atoms within the silicon–oxygen network. Elevated Ca^{2+} content promotes its incorporation into tetrahedral sites or interstitial positions, disrupting network continuity and enhancing inter-segment interactions—thereby increasing viscosity. Second, under high-calcium conditions, the clinker tends to form $C_{12}A_7$—a phase with high hydration activity and strong water affinity. Its presence reduces free water content in the past, further contributing to the observed viscosity increase.

3.3.2 Slurry fluidity

Figure 7 illustrates the effects of calcination temperature and Ca/Si ratio on slurry fluidity. In the range of 600–800 °C, fluidity initially decreases and then increases with temperature, reaching a maximum of 231 mm at 800 °C. This trend is primarily attributed to the optimal excitation of coal gangue at 800 °C, which significantly accelerates hydration, rapidly consuming free water and increasing internal resistance—thereby

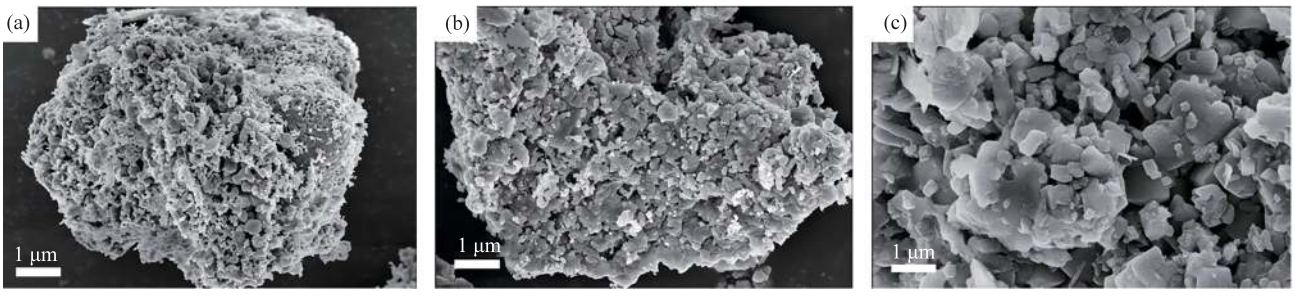

Figure 5 SEM images of clinker under different Ca/Si molar ratios: (a) 1.5, (b) 2.0, and (c) 2.5

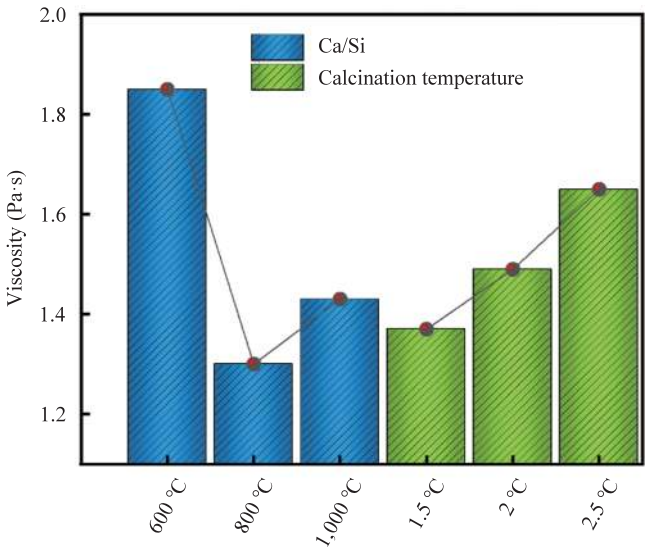

Figure 6 Viscosity of paste with different calcination temperatures and Ca/Si ratio

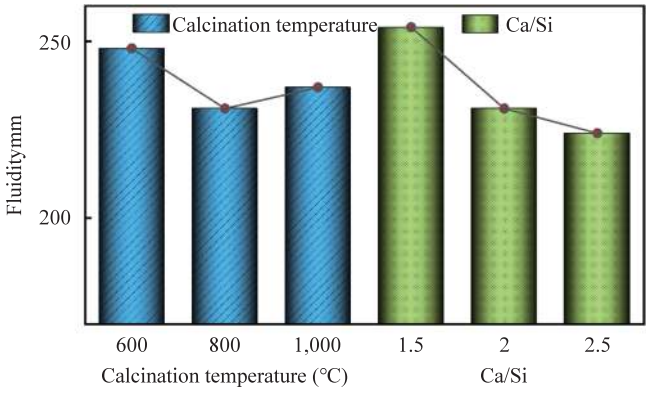

Figure 7 Fluidity test bar chart

reducing fluidity. At 1,000 °C, fluidity further rises to 242 mm. The diminished excitation effect at this temperature slows hydration, preserving higher free water content and thus enhancing fluidity.

As shown in Figure 7, slurry fluidity decreases monotonically from 254 to 224 mm as the Ca/Si molar ratio increases from 1.5 to 2.5. This trend is governed by two factors. On one hand, at Ca/Si = 1.5, the relatively weak activation of coal gangue precludes the formation of highly hydraulic $C_{12}A_7$ in the clinker, resulting in lower free water consumption and thus higher fluidity. On the other hand, when Ca/Si reaches 2.5, excessive f-CaO appears in the system; its rapid hydration further consumes free water, exacerbating fluidity loss [27].

3.3.3 Slurry setting time

Figure 8 illustrates the influence of calcination temperature and Ca/Si ratio on the setting time of CGCM. As calcination temperature increases, both initial and final setting times initially shorten and then prolong, reaching minima at 800 °C—175 and 224 min, respectively. This trend is attributable to two factors. On one hand, elevated calcination temperature enhances the amorphization of kaolinite, quartz, and other phases in the precursor, increasing their reactivity. This enables faster reaction with water during hydration, accelerating the formation of C–S–H, C–A–S–H, and other hydration products, thereby shortening setting time; The minimum setting time at 800 °C is further attributed to the abundance of mayenite ($C_{12}A_7$)—a highly hydraulic, rapid-setting phase (Section 4.2.1). Conversely, at 1,000 °C, the formation of gehlenite (C_2AS), characterized by its stable structure and poor hydraulicity, markedly delays hydration and prolongs setting.

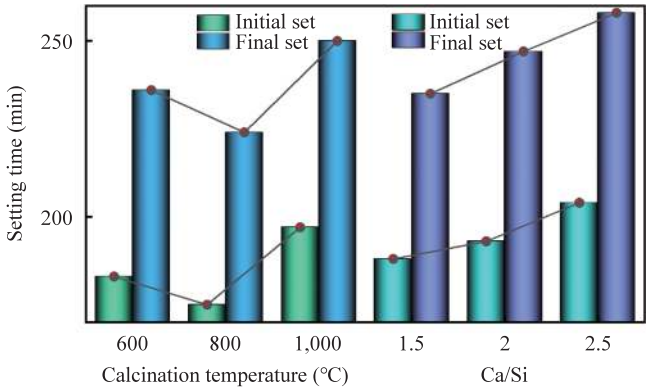

Figure 8 Setting time with different calcination temperatures and Ca/Si ratios

As the Ca/Si molar ratio increases from 1.5 to 2.5, both initial and final setting times of the cementitious material progressively shorten, reaching 204 and 258 min, respectively, at Ca/Si = 2.5. This trend is primarily attributed to two factors. First, as discussed in Section 4.1.2, higher Ca/Si favors the formation of high-calcium aluminate $C_{12}A_7$ in the clinker—a phase that hydrates rapidly and effectively accelerates setting. Second, elevated Ca/Si increases the content of f-CaO in the clinker, which reacts during hydration

to form calcium hydroxide and release heat, further promoting early hydration and condensation, thereby shortening setting time.

3.3.4 Pozzolanic activity

Figure 9 illustrates the influence of calcination temperature on the electrical conductivity and pH of CGCM. As shown in Figure 9(a), ion dissolution and consumption behaviors vary markedly with temperature. At 600 °C, conductivity exhibits the most gradual evolution: it decreases from 30 to 80 min, increases from 80 to 150 min, and subsequently stabilizes. This pattern is attributed to incomplete carbon combustion in coal gangue at this temperature; residual carbon encapsulates active components, hindering the dissolution of Ca^{2+} and OH^- and thereby suppressing conductivity. As hydration proceeds, progressive exposure of active phases releases Si^{4+}, Al^{3+}, and Ca^{2+} ions, contributing to late-stage conductivity. At a calcination temperature of 800 °C, conductivity exhibits a broader variation range with mild oscillations and distinct inflection points at 40, 60, 120, and 180 min (Figure 9(a)). The sharp decline within the first 40 min reflects rapid ion consumption during intense hydration, primarily forming C–S–H gels. The partial recovery observed between 40 and 60 min is likely attributable to continued hydration of residual f-CaO, which releases additional OH^- ions.

Figure 10 illustrates the influence of Ca/Si ratio on the conductivity and pH of coal gangue-based cementitious materials. As shown in Figure 10(a), at Ca/Si ratios of 1.5 and 2.0, conductivity remains relatively stable, indicating a dynamic equilibrium between ion dissolution and consumption. The system with Ca/Si = 2.0 exhibits higher overall conductivity, attributed to enhanced release of Ca^{2+} and OH^- from its elevated

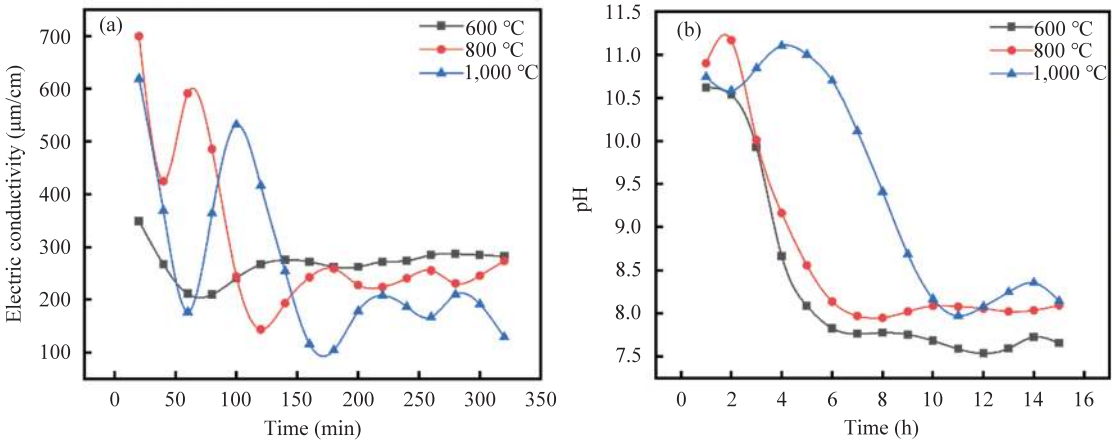

Figure 9 Variation pattern of conductivity and pH with calcination temperature

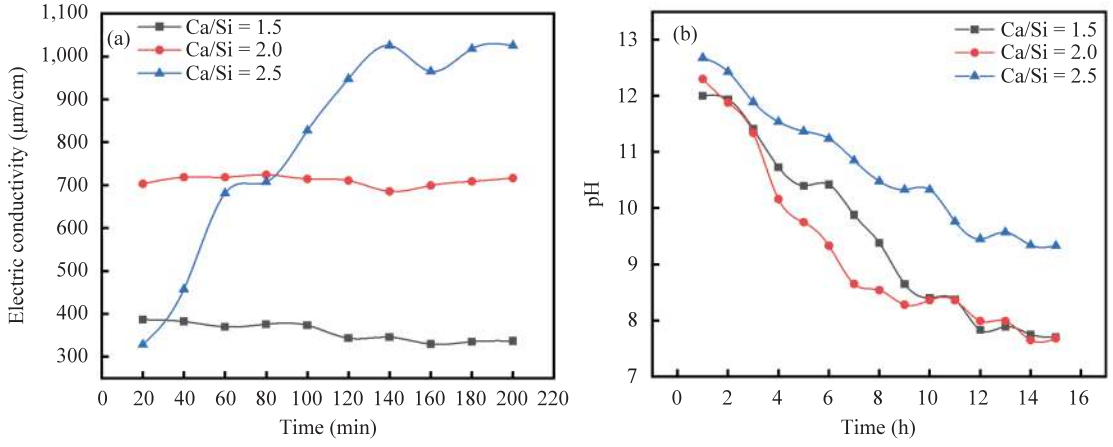

Figure 10 Variation pattern of conductivity and pH with calcination temperature

calcium content. In contrast, when Ca/Si increases to 2.5, conductivity exhibits a distinct two-stage "rapid rise–stabilization" pattern. A sharp increase occurs between 80 and 140 min, driven by rapid hydration of active phases that release Ca^{2+} and OH^-, thereby raising ionic concentration and mobility. Subsequently, stabilization occurs as hydration products form, establishing equilibrium between ion dissolution and consumption. Figure 10(b) demonstrates that the Ca/Si ratio governs pH evolution by modulating alkalinity and pozzolanic reactivity. At Ca/Si = 1.5, limited Ca^{2+} and OH^- availability results in a low initial pH. At Ca/Si = 2.0, the Ca^{2+} to dissolved Si–Al species ratio approaches an optimum, triggering intense pozzolanic reactions. The rapid consumption of OH^- during C–S–H and C–A–H formation induces a sharp pH decline after a brief initial rise—indicative of peak reactivity. At Ca/Si = 2.5, initial pH reaches its maximum; however, excess Ca^{2+} forms a passivation layer on particle surfaces, inhibiting further dissolution. Concurrently, limited silica availability restricts OH^- consumption, resulting in sustained high pH with minimal decline.

4 Conclusion

This study demonstrates the feasibility of converting coal gangue into high-performance cementitious materials via synergistic hydrothermal–low-temperature calcination, and elucidates the mechanisms by which key parameters govern microstructural evolution and macroscopic properties. The main conclusions are as follows:

(1) Orthogonal experiment results establish the following order of factor significance for 28-day compressive strength of CGCM: calcination temperature > Ca/Si molar ratio > hydrothermal temperature > NaOH content. The optimal process parameters—hydrothermal temperature of 90 °C, Ca/Si = 2.0, NaOH content of 1.5%, and calcination temperature of 800 °C—yield a 28-day compressive strength of 19.3 MPa.

(2) Calcination temperature emerges as the most critical factor governing CGCM performance. At 800 °C, the clinker develops highly active phases—β-C_2S, α'H-C_2S, CA, and $C_{12}A_7$—alongside a porous microstructure that facilitates ion migration and hydration product growth, thereby significantly enhancing cementitious properties. Conversely, temperatures below or above this optimum impair performance: lower temperatures leave residual carbon that hinders reactivity, while 1,000 °C promotes inert gehlenite (C_2AS) formation, degrading activity.

(3) The Ca/Si ratio governs cementitious perfo-rmance by modulating silicate network polymerization and active phase formation. At Ca/Si = 2.0, an optimal balance is achieved between promoting $C_{12}A_7$ generation and reducing silicon–oxygen network connectivity, thereby maximizing gelation activity. Conversely, excessive Ca/Si leads to f-CaO enrichment, which introduces structural defects and inhibits further reaction.

(4) The CGCM paste exhibits a viscosity of 1.34 Pa·s, fluidity of 231 mm, and setting times of 175 min (initial) and 224 min (final)—all meeting the workability requirements for mine backfilling and similar technical applications.

Acknowledgements

This work was supported by the Shanxi Province Key Laboratory Construction Project Funds (Grant No. 202104010910021), the General Project of Shanxi Province Basic Research Program (Grant No. 202303021211061), the General Program of the National Natural Science Foundation of China (Grant No. 52474140), the Key Program of the National Natural Science Foundation of China (Grant No. 52334005), the Regional Joint Key Project of the National Natural Science Foundation of China (Grant No. U22A20151), the New Cornerstone Science Foundation through the XPLORER PRIZE, and the Ten Thousand Talent Program of China for Leading Scientists in Science, Technology, and Innovation.

Conflict of interest

The authors declare that they have no conflict of interests.

Data availability

The relevant data are available from the authors upon reasonable request.

References

[1] Q. Song, T. Song, J. Nie, H. Zhou, Y. Hu, Y. Chen, Y. Deng, Q. He, and F. Cheng, "An investigation on the use of coal gangue and coal gasification slag as reducing agent in synergistic utilization of steel slag for higher-activity supplementary cementitious materials," *Construction and Building Materials*, vol. 477, p. 141094, 2025.

[2] D. Li, Y. Fan, X. Dong, X. Ma, W. Wu, W. Xiao, and M. Yang, "Effects of carbonaceous and ash synergism on the properties of coal mine solid waste filler materials: modulation of hydration mechanisms, strength generation mechanisms, and fine-scale damage," *Journal of Cleaner Production*, vol. 519, p. 145797, 2025.

[3] L. Wang, Q. Wang, J. Cai, F. Zhou, Z. Cheng, and J. Zhang, "Experimental study on the mechanical properties and microstructural mechanisms of coal gangue-based cementitious materials synergistically activated by desulfurization gypsum and lime," *Polymers*, vol. 17, no. 7, p. 932, 2025.

[4] N. Zhang, H. X. Li, and X. M. Liu, "Hydration kinetics of cementitious materials composed of red mud and coal gangue," *International Journal of Minerals, Metallurgy, and Materials*, vol. 23, no. 10, pp. 1215–1224, 2016.

[5] J. Li, X. Liu, C. Cai, Q. Su, M. Chen, and X. Zhu, "From waste to value: Engineering properties and failure mechanisms of green backfills utilizing molybdenum tailings, fly ash and coal gangue," *Powder Technology*, vol. 464, p. 121294, 2025.

[6] J. Qiu, T. Zhang, L. Li, Y. Huo, T. Lei, and Y. Liu, "Improvement of mechanical properties and frost resistance of coal gangue concrete: synergistic effect and microscopic mechanism of basalt fiber, fly ash and silica fume," *Journal of Cleaner Production*, vol. 522, p. 146324, 2025.

[7] Q. Zhang, X. Zhang, L. Wang, and S. Zhang, "Synthesis, characterization, and cementitious activity of the magnesium silicate hydrate and calcium silicate hydrate from coal gangue," *Molecules*, vol. 30, no. 8, p. 1725, 2025.

[8] H. Guo, H. Wang, H. Li, H. Xue, L. Wei, Y. Li, Y. Chen, Q. Li, and H. Dong, "Comparison of performance, hydration behavior, and environmental benefits of coal gangue cementitious materials prepared by wet and dry grinding methods," *Construction and Building Materials*, vol. 471, p. 140665, 2025.

[9] Q. Gao, S. Jiu, Y. Chen, S. Zhao, C. Chen, and R. Jia, "Modification of low-quality calcined coal gangue and its effect on mechanical properties and microstructure," *Construction and Building Materials*, vol. 458, p. 139433, 2025.

[10] G. Dou, C. Wang, X. Zhong, and B. Qin, "Preparation and characterization of green lignin modified mineral cementitious firefighting materials based on uncalcined coal gangue and coal fly ash," *Construction and Building Materials*, vol. 435, p. 136799, 2024.

[11] Y. Jin, L. Li, Z. Liu, S. Zhu, and D. Wang, "Synthesis and characterization of low-cost zeolite NaA from coal gangue by hydrothermal method," *Advanced Powder Technology*, vol. 32, no. 3, pp. 791–801, 2021.

[12] S. Wang, X. Peng, L. Tang, L. Zeng, and C. Lan, "Influence of hydrothermal synthesis conditions on the formation of calcium silicate hydrates: from amorphous to crystalline phases," *Journal of Wuhan University of Technology-Mater. Sci. Ed.*, vol. 33, no. 5, pp. 1150–1158, 2018.

[13] Z. Yang, D. Kang, D. Zhang, C. Yan, and J. Zhang, "Crystal transformation of calcium silicate minerals synthesized by calcium silicate slag and silica fume with increase of C/S molar ratio," *Journal of Materials Research and Technology*, vol. 15, pp. 4185–4192, 2021.

[14] D. Kong, T. Wang, J. Zhang, T. Li, and T. Liu, "Improvement of strength and microstructure of low-carbon cementitious materials with high volume of calcined coal gangue," *Construction and Building Materials*, vol. 444, p. 137916, 2024.

[15] X. Zhang, S. Zhu, T. Yang, Y. Wang, J. Li, and K. Li, "The influence of coal gangue dosage and concentration on the properties and hydration mechanism of fly ash-based cemented filling materials," *Journal of Cleaner Production*, vol. 492, p. 144903, 2025.

[16] B. Liu, X. Gu, Z. Li, B. Yang, H. Wang, J. Liu, M. L. Nehdi, and Y. Zhang, "Exploring microwave activation as a novel method for activating coal gangue: Focus on microwave activation mechanisms and hydration characteristics of cementitious supplementary materials," *Construction and Building Materials*, vol. 450, p. 138482, 2024.

[17] Y. Gong and Y. Fang, "Preparation of belite cement from stockpiled high-carbon fly ash using granule-hydrothermal synthesis method," *Construction and Building Materials*, vol. 111, pp. 175–181, 2016.

[18] F. N. Bouha, L. Kacimi, and G. Angeles, "Manufacture of rich-sulfoaluminate belite cement at low temperature from waste mixture by dry and hydrothermal processes," *Construction and Building Materials*, vol. 314, p. 125641, 2022.

[19] A. Rungchet, P. Chindaprasirt, S. Wansom, and K. Pimraksa, "Hydrothermal synthesis of calcium sulfoaluminate–belite cement from industrial waste materials," *Journal of Cleaner Production*, vol. 115, pp. 273–283, 2016.

[20] K. Baltakys, T. Dambrauskas, D. Rubinaite, R. Siauciunas, and A. Grineviciene, "Formation and hydration of eco-friendly cement using industrial wastes as raw materials," *Scientific Reports*, vol. 11, no. 1, p. 14742, 2021.

[21] J. Koplík, J. Švec, J. Másilko, M. Sedlačík, and E. Bartoníčková, "Synthesis of calcium aluminate hydrates, their

characterization and dehydration," *Ceramics International*, vol. 51, no. 5, pp. 5536–5543, 2025.

[22] S. Maheswaran, S. Kalaiselvam, S. S. Karthikeyan, C. Kokila, and G. S. Palani, "β-Belite cements (β-dicalcium silicate) obtained from calcined lime sludge and silica fume," *Cement and Concrete Composites*, vol. 66, pp. 57–65, 2016.

[23] T. Qi, X. Gao, G. Feng, J. Bai, Z. Wang, Q. Chen, H. Wang, and X. Du "Effect of biomass power plant ash on fresh properties of cemented coal gangue backfill," *Construction and Building Materials*, vol. 340, p. 127853, 2022.

[24] Y. Vanhove, J. G. Dossa, J. Page, and C. Djelal, "Rheological benefits of biomass fly ash as filler replacement in cement-based materials," *Case Studies in Construction Materials*, vol. 22, p. 04133, 2025.

[25] J. Xiang, J. Qiu, Y. Zhao, P. Zheng, H. Peng, and X. Fei, "Rheology, mechanical properties, and hydration of synergistically activated coal gasification slag with three typical solid wastes," *Cement and Concrete Composites*, vol. 147, p. 105418, 2024.

[26] J. Xin, L. Liu, L. Xu, J. Wang, P. Yang, and H. Qu, "A preliminary study of aeolian sand-cement-modified gasification slag-paste backfill: Fluidity, microstructure, and leaching risks," *Science of The Total Environment*, vol. 830, p. 154766, 2022.

[27] Y. Wan, Y. Guo, C. Li, X. Li, and G. Feng, "Synthesis use of coal gasification slag to prepare belite sulphoaluminate cementitious material and its hydration characteristics study," *Construction and Building Materials*, vol. 467, p. 140370, 2025.

[28] M. Zhang, L. Li, F. Yang, S. Zhang, H. Zhang, and J. An, "Thermal activation and mechanical properties of high alumina coal gangue as auxiliary cementitious admixture," *Materials Research Express*, vol. 11, no. 2, p. 025201, 2024.

[29] M. Zhang, L. Li, F. Yang, S. Zhang, H. Zhang, and J. An, "Thermal activation and mechanical properties of high alumina coal gangue as auxiliary cementitious admixture," *Materials Research Express*, vol. 11, no. 2, p. 025201, 2024.

[30] S. Sui, X. Kong, S. Li, H. Wang, D. Liu, S. Gao, Y. Geng, J. Chen, and X. Chen, "Impact of Low-Activity Coal Gangue on the Mechanical Properties and Microstructure Evolution of Cement-Based Materials," *Buildings*, vol. 15, no. 17, p. 3073, 2025.